

# Approaching ballistic transport in suspended graphene

Xu Du, Ivan Skachko, Anthony Barker, Eva Y. Andrei

*Department of Physics & Astronomy, Rutgers the State University of New Jersey*

## **Supplementary Information**

### *Contents*

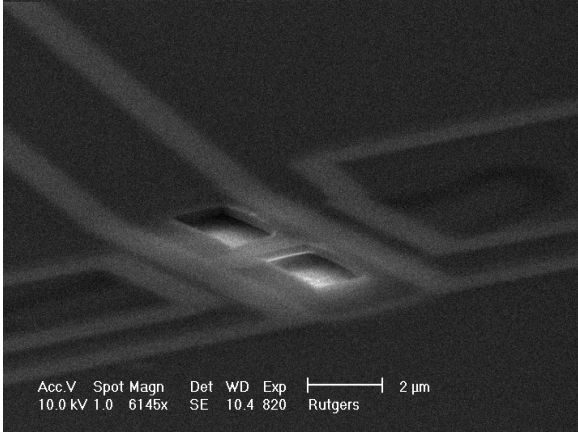
- A. Graphene preparation
- B. Suspending the graphene device
- C. Measurements
- D. Impact of lead geometry

### **A. Graphene preparation**

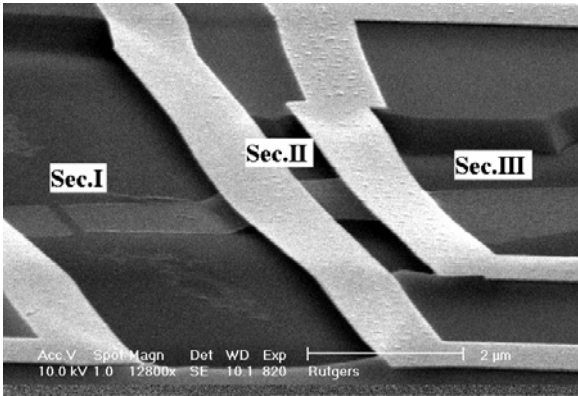
Graphene deposition is done using a method similar to the one introduced by the pioneering work in ref. S1. Prior to graphene deposition, the Si/SiO<sub>2</sub> substrates were baked in forming gas (Ar/H<sub>2</sub>) at 200C for 1 hour to remove water and organic residue. A thin foil of highly oriented pyrolytic graphite (neutron detector quality) was peeled from the bulk material using scotch tape and transferred onto the Si/SiO<sub>2</sub> substrate with a fine pair of tweezers. Pressure was then applied onto the graphite foil using compressed high purity nitrogen gas through a stainless steel needle, for ~5 seconds. The foil was then removed from the substrate and the substrate was carefully checked under an optical microscope for candidates of single layer graphene. This process is repeated until a few graphene flakes can be identified. The sample was then immediately coated with PMMA resist for further E-beam lithography.

## ***B. Suspending the graphene device***

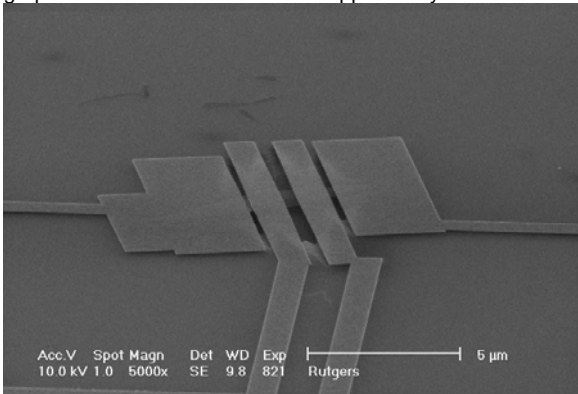
The suspended graphene (SG) devices were fabricated from conventional non-suspended graphene (NSG) devices with Au/Ti leads deposited on Si/SiO<sub>2</sub> (300nm) substrates. After the NSG devices were made, the samples were coated with PMMA. And an additional e-beam lithography step was carried out to open two small PMMA windows (typically 0.2 ~ 0.5µm squares) on the two sides of the graphene channel (illustrated in Figure1). The samples were then immersed in 7:1 (NH<sub>4</sub>F: HF) buffered oxide etch. Etching was done at 25C<sup>0</sup> for 6.5 min. Due to the weak coupling of graphene to the substrate, capillary action draws the etchant underneath the whole graphene film. Hence, the etching actually starts in the entire graphene channel shortly after the sample is immersed. The isotropic etching therefore results in the whole device (the graphene and the leads attached to it) to become suspended (Figure 2). After the etching, the etchant was replaced by DI water, then hot acetone (to remove the PMMA) and finally hot isopropanol, with the sample remaining the liquid at all times. Finally the sample was taken out of the isopropanol and left to dry. Normally the suspended device would be destroyed by wicking of the liquid at this point. However due to the small surface tension of hot isopropanol, devices with channel length smaller than 1µm were found to survive the process with high success rate (Figure 3). The SG samples were baked in forming gas (Ar/H<sub>2</sub>) at 200C<sup>0</sup> for 1 hour to further remove organic residue and water right before the measurements.



**Supplementary Figure 1.** SEM image of a SG device in the middle of its fabrication process. The sample, started from a conventional device on substrate, was coated with PMMA. 2 holes were opened at the sides of the graphene channel in PMMA mask. The BOE etch removes the SiO<sub>2</sub> underneath the device, and (before the removal of the PMMA) creates a PMMA bridge which protects the graphene from been collapsed by the surface tension. In the fabrication of the actual devices, the samples were left in liquid without taken out until the PMMA mask is removed.



**Supplementary Figure 2.** SEM image of the same device shown in Figure 1. This figure illustrates the possible problems one may encounter during the fabrication of a SG device. Section I: the graphene bridge was too long (~3 μm), hence got torn apart by the surface tension when the solvent dried out. Section II: a short section of graphene which was successfully suspended. The gold leads were significant sagged by the surface tension, due to the reduced mechanical strength as a result of over etching and over broadening of the ditch (this device was etched for 10 min). Section III: without support from the leads, graphene collapsed onto the back gate. For actual working devices, the edge of the graphene has to be covered and supported by the leads.



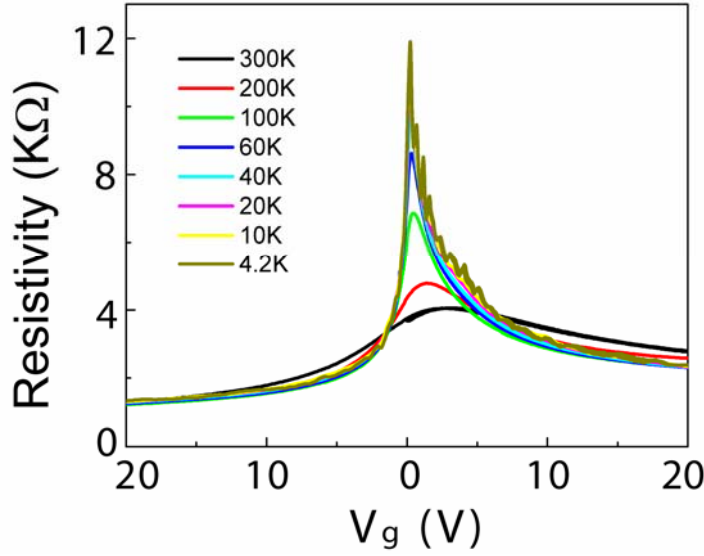
**Supplementary Figure 3.** SEM image of a working SG device. The channel length between the voltage leads is ~0.6 μm. The etching time is 6.5 min.

### **C. Measurements**

The transport properties of the SG samples were measured with a standard 4-probe lock-in technique, using a 17Hz 100nA excitation current. To prevent bending of graphene from electrostatic force and breakdown of the gas dielectric (helium exchange gas), we limit the gate voltage to a range of  $\pm 20V$ .

Figure 4 shows the gate voltage dependence of resistivity at various temperature from 300K to 4.2K, for a SG device ( $L=0.6\mu\text{m}$ ,  $W=1.6\mu\text{m}$ ). The asymmetry between the electron and hole branches revealed by the  $\rho(V_g)$  curves was observed in all the SG devices we fabricated thus far. We also observed the asymmetry in NSG samples with similar geometry (voltage leads placed across the current path) for short lead separation ( $L < 1 \mu\text{m}$ ). We find that the asymmetry decreases with increasing lead separation and becomes quite small in samples with the largest separation or when the voltage leads are placed in a non-invasive manner (such as in the Hall bar geometry). This suggests a link between the asymmetry and the presence of the leads. However, the mechanism by which the leads can introduce such asymmetry is still poorly understood. Some possible scenarios include: contamination associated with the deposition of leads; doping at the contact between the metal and graphene, which may alter the Density of states on one of the carrier branches; a geometrical effect associated with the boundary conditions imposed by the voltage leads. A detailed study of the effect of leads will be undertaken in the future.

At low temperatures ( $T < 20K$ ), oscillation in  $\rho(V_g)$  were observed. These oscillations are due to interference of carriers bouncing back and forth between the leads with wavelength tuned by the gate voltage.



**Supplementary Figure 4.** Gate voltage dependence of resistivity at various temperature indicated in the legend, for a SG device with  $L=0.6 \mu\text{m}$ ,  $W=1.6 \mu\text{m}$ .

#### **D. Impact of lead geometry**

The geometry of the voltage leads imposes the boundary conditions on the electronic wavefunctions and therefore it is one of the most important factors in the measured mobility of near-ballistic samples. In the case of ideal ballistic junctions measured in a 2-lead geometry, the conductance is controlled by the transmission probabilities,  $T_n$ , of the allowed electronic modes which are defined by the boundary conditions (Tworzydło, J. et. al., PRL. 96, 246802 (2006)):

$$\sigma = \frac{L}{W} \frac{4e^2}{h} \sum_n T_n \quad (1)$$

here:

$$T_n = \left| \frac{k_n}{k_n \cos(k_n L) + i \frac{\mu}{\hbar v_F} \sin(k_n L)} \right|^2 \quad (2)$$

where  $k_n = \sqrt{\left(\frac{\mu}{\hbar v_F}\right)^2 - (q_n)^2}$ ,  $q_n = \frac{1}{W} \pi(n+1/2)$ , and  $W$  is the width of the junction.

When  $k_n$  is imaginary, the modes are evanescent and the transmission is negligible, so we only consider the terms where  $k_n$  is real, hence  $\frac{\mu}{\hbar v_F} > q_n$ , or  $n < \frac{\mu W}{\hbar v_F \pi}$ .

With  $k_n$  being real,

$$T_n = \frac{\mu^2 - (\hbar v_F q_n)^2}{\mu^2 - (\hbar v_F q_n)^2 \cos^2(k_n L)} \quad (3)$$

hence:

$$\begin{aligned} \sigma &\sim \frac{L}{W} \frac{4e^2}{h} \sum_{n=0}^{\text{int}\left(\frac{\mu W}{\hbar v_F \pi}\right)} \frac{\mu^2 - (\hbar v_F q_n)^2}{\mu^2 - (\hbar v_F q_n)^2 \cos^2(k_n L)} \\ &\sim \frac{L}{W} \frac{4e^2}{h} \frac{\mu W}{\pi \hbar v_F} \int_0^1 \frac{1-x^2}{1-x^2 \cos^2\left(\frac{\mu L}{\hbar v_F} \sqrt{1-x^2}\right)} dx \end{aligned} \quad (4)$$

here  $x = \frac{\pi \hbar v_F}{\mu W} (n + 1/2)$ .

For large  $\frac{\mu L}{\hbar v_F}$ , the integral in equation (4) approaches  $\frac{\pi}{4}$ , which yields:

$$\sigma \sim \frac{e^2}{h} \frac{L\mu}{\hbar v_F}$$

comparing with the semiclassical Boltzmann result:  $\sigma = \frac{e^2 v_F^2 N(E_F) \tau}{2}$ , we obtain the

mean free path  $mfp = v_F \tau \sim L/2$ .

Thus the boundary conditions limit the mean free path of the device to  $1/2$  the lead

separation. This result is almost independent of the Fermi energy except at the Dirac

point, as demonstrated in the more precise numerical calculations shown in

supplementary Figure 5a. Consequently, the mobility of ballistic 2-lead devices is finite

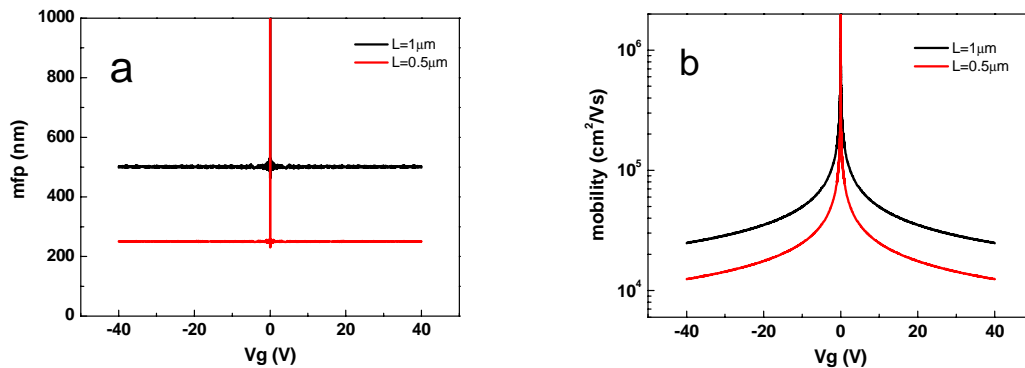
and reflects a ‘‘device mobility’’ which depends on gate voltage as  $\mu \propto V_g^{-1/2}$  ( shown in

supplementary Figure 5b). By contrast, for junctions measured in a Hall-bar geometry,

the mean free path is not limited by the voltage leads so the mobility usually measures the

‘‘perfection’’ of the material, or the ‘‘material mobility’’.

In our devices, the voltage leads run across the width of the sample (2-lead geometry) to provide structural support for the suspended graphene. Therefore, the measured mobility in our suspended graphene devices reflects the “device mobility”. Its value is affected by the disorder in graphene but it is bounded by the value imposed by the voltage lead separation. This is supported by the observed gate voltage dependence of the mobility in our geometry. When the lead separation in a 2-lead measurement is much smaller than the mean free path of the material, the measured mobility is the “device mobility” and does not give access to the material-limited mobility. In the opposite limit, when the lead separation is much larger than material mfp, the measurement does probe the material mobility. The experiments described here are at the crossover between the two limits. While the two lead geometry does not give a direct measure of the material-limited mobility, it does provide experimental access to the physics of the 2D Dirac Fermion system, including geometrically defined modes and interference effects, which have thus far only been addressed theoretically.



**Supplementary Figure 5.** Numerically calculated gate voltage dependence of mobility and mfp for ideal ballistic junctions with indicated geometries, for graphene junctions on 300nm SiO<sub>2</sub>.

## ***Supporting Reference***

S1. K.S. Novoselov *et.al.*, *Science* **306**, 666 (2004)